Design of Self-Starting Hybrid Axial Flux Permanent Magnet Synchronous Motor Connected Directly to Line

Mustafa Eker*, Mehmet Akar[†], Cem Emeksiz*, Zafer Dogan*
and Ahmet Fenercioglu*

Abstract – In view of the current state of the reserves of electric energy generated resources and the share of electric motors in electricity consumption, many researches and studies related to efficiency in electric motors are being made. The presented work is related to the Axial Flux Permanent Magnet Synchronous Motor (AF-PMSM), which has recently undergone significant work based on the development of magnet and motor technology. In this study, a novel AF-PMSM was designed analytically through Finite Element Method (FEM) which can be started by connecting to a line such as an asynchronous motor in a transient state and can operate with high efficiency and power factor after synchronization in steady state without the need for an expensive motor drive. According to the obtained FEM results, a design with an efficiency class of IE4 of 5.5 kW shaft power, a 4 poles motor was obtained. As a result, economic calculations indicate that the extra cost of the designed Line start AF-PMSM with respect to the asynchronous motor is rapidly compensated by energy saving due to a more efficient operation, especially constant speed operations. As a result of the analysis obtained, the targeted values are reached. For induction motors and radial flux permanent magnet synchronous motors, a good alternative motor that can operate with high efficiency and power factor has been obtained.

Keywords: Line Start, Axial Flux, PMSM, FEM

1. Introduction

In the recent years, many studies have dealt with the usage and conservation of energy resources. Use of energy as well as the current state of the reserve energy source is very important. Electric motors constitute a significant share of the use of energy. For this reason, today's electric motor manufacturers/users are obliged to manufacture/use more efficient motors.

In electricity consumption, the share of electric motors and the systems they use is high. Therefore, the efficiency of the used motors is crucial. [1, 2]. There are also legal arrangements on efficiency in electric motors [2-4]. The legal classification used today is made by the International Electrotechnical Commission (IEC). Fig. 1 includes the graphic of these classifications [4].

Considering the usage rates of motors, asynchronous motors are preferred 70%-75% more due to their simple structure, lower manufacturing cost and reliable operation. With production of rare earth permanent magnets (PM), the use of PM motors in the industry has increased. These motors cannot be directly connected to the line. In order to provide a line start, it is necessary to modify the structure

of the rotor [5]. There are various studies conducted on PM motors' starting and synchronizing, torque ripple, magnet structure and properties [6]. Another alternative to the radial flux motor is axial flux motors. In many modern industrial applications, AF-PMSM has the required features of electrical machines such as high efficiency, high power density, brushless and able to regulate air gap flux density under a wide range of load conditions [7, 8].

In this study, an axial-flux permanent magnet synchronous motor is designed, which will take the place of asynchronous motors especially in constant speed applications and can be connected directly to the line with IE4 efficiency class.
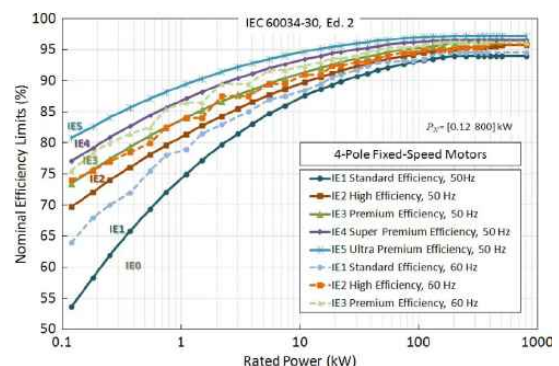

Fig. 1. Revised version of IEC 60034-30 efficiency classification standard, representing classes from IE1 to IE5 for four-pole electric motors

† Corresponding Author: Dept. of Mechatronics Engineering, Gaziosmanpasa University, Turkey. (mehmet.akar@gop.edu.tr)
* Faculty of Engineering and Natural Sciences, Gaziosmanpasa University, Turkey. ({mustafa.eker, cem.emeksiz, zafer.dogan, ahmet.fenercioglu}@gop.edu.tr)
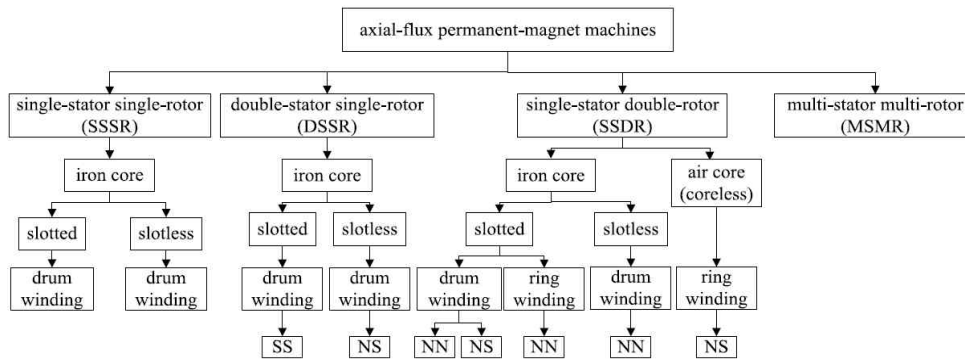
Fig. 2. AFPM machine topologies

Due to its simple structure, easy manufacturing and high torque capacity, a single rotor single stator structure is preferred. The originality of this study is that the squirrel cage is added to the rotor that provides line start like an asynchronous motor during the start and working with high efficiency and constant speed like PMSMs in steady state because it does not have rotor electrical and magnetizing loses. Another important advantage of this design is that it eliminates the need for a high-performance driver to operate PMSM-type motors.

The present study consists of 4 chapters. The first part is Introduction. In the second part, general information about Line Start AF-PMSM is given. The third part is the Design and Result section in which the simulation work and the results are included. Finally, Conclusions part is presented.

2. Line Start AF-PMSM

The structure that will be an alternative to radial-flux permanent magnet motors is the axial flux permanent magnet motor structure. Due to advantages of AF-PMSM increase the popularity of these motors [9-11]. AFPMs are produced in different topologies. These topologies have different names depending on the number of stators and rotors, the stator slot structure, the positioning of the magnets and the winding structure as can be seen in Fig. 2 [12, 13].

AF-PMSM classifications based on the number of stators and rotors are particularly useful in grading classifications [14]. AF-PMSM topologies have advantages and dis-advantages in comparison to other topologies [15-18].

In this study, single-sided (single stator-single rotor) structure is used. This structure is considered as the simplest structure. It has a high torque capacity and is therefore often preferred in military transport, servo electromechanical drives and non-geared lift systems [15]. This structure also forms the basis of structures such as Kaman and Torus [14].

2.1 AF-PMSM design equations

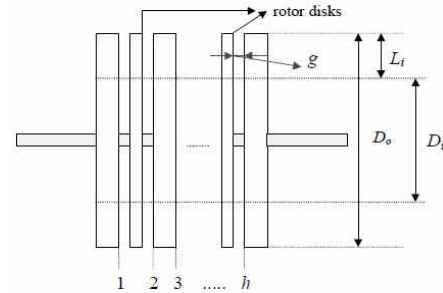The design of the stator and rotor of the axial flux motor

Fig. 3. Generalized representation for AFSM

is based on the cylindrical structure of the induction and synchronous motor, a standard throughout the world. The obtained parameters are calculated by considering the axial structure of the rotor and stator inner diameter, outer diameter and thickness by the method of calculation of constant magnetic circuit [19]. Different topologies are mentioned for AFSM. AFSM's generalized representation is given in Fig. 3 [20].

In Fig. 3; D_0, D_i, L_i, g and h represent the stator outer diameter, the inner diameter, the effective length in the stator radial direction, the air gap length and the stator number respectively. Other important parameters for the AFSM are the stator average diameter (D_{av}) and pole pitch at the average diameter (τ) [20].

$$D_0 = \sqrt[3]{\frac{\varepsilon P_{out}}{\pi^2 k_D k_{\omega 1} n_s B_{mg} A_m \eta \cos\varphi}} \tag{1}$$

$$D_i = k_D D_0 \tag{2}$$

$$D_{av} = 0.5(D_0 + D_i) \tag{3}$$

$$\tau = \frac{\pi D_{av}}{2p} \tag{4}$$

In the given equation ε represents the phase EMF-to-phase voltage ratio, P_{out} represents shaft power, k_D is coefficient based on D_i / D_o, $k_{\omega 1}$ represents the winding factor, n_s represents rotor speed, B_{mg} represents peak value of magnetic flux density in the air gap, A_m represents peak value of the line current density, η represents efficiency and $\cos\varphi$ is power factor. k_d is ratio of inner

diameter to outer diameter of stator [21].

If the induced current in the air gap is assumed to be sinusoidally distributed due to the stator current, then the total current of each phase and three phases are as follows [20]:

$$
\left\{
\begin{array}{l}
PhaseA: \quad \hat{i}\cos\omega t \dfrac{N_s}{2}\sin p\theta d\theta \\[2mm]
PhaseB: \quad \hat{i}\cos\left(\omega t - \dfrac{2\pi}{3}\right)\dfrac{N_s}{2}\sin\left(p\theta - \dfrac{2\pi}{3}\right)d\theta \\[2mm]
PhaseC: \quad \hat{i}\cos\left(\omega t + \dfrac{2\pi}{3}\right)\dfrac{N_s}{2}\sin\left(p\theta + \dfrac{2\pi}{3}\right)d\theta
\end{array}
\right\}
\quad (5)
$$

$$
\frac{3}{2} I \sqrt{2}\, \frac{N_s}{2}\sin\left(p\theta - \omega t\right)d\theta \qquad (6)
$$

I is the rms value of the current, and $\hat{i}$ is the peak value of current. N_s is series turns, p is the number of pole pairs. The basic component $B_{g1}(\theta)$ of air-gap flux density produced by the magnets is given in Eq. (7) [20].

$$
B_{g1}(\theta) = \hat{B}_{g1}\cos(p\theta - \omega t - \alpha) \qquad (7)
$$

$\hat{B}_{g1}$ is the amplitude of the basic component. α represents the electrical angle between the stator and rotor magnetic axis. If the relevant equations are set, the value of the basic torque component for a single stator is as follows [20]:

$$
T_1 = \frac{3}{8}\sqrt{2}\pi\hat{B}_{g1}N_s I\left(r_0^2 - r_i^2\right)\sin(\beta) \qquad (8)
$$

The r_0 and r_i in the torque equation represents the outer and inner radius of the stator, and $\beta - \alpha$ represents the angle known as the torque angle in the synchronous machine. In fact, sinusoidal placement of all of the windings is almost impossible. In this case [20]:

$$
N_s = \frac{4}{\pi}k_{\omega1}N_{ph} \qquad (9)
$$

In the given equation N_{ph} represents the number of series windings per phase. In the same way, the torque equation can also be defined in terms of the average diameter and effective length [20].

$$
T_1 = \frac{3}{2}\sqrt{2}\pi\hat{B}_{g1}k_{\omega1}N_{ph}I D_{av}L_i\sin(\beta) \qquad (10)
$$

To simplify design formulas, the coefficient K_1 known as stator surface current density or specific electrical charge is often added. This value is generally around 10000 A/m for small power motors and around 40000 A/m for medium power motors [20]:

$$
K_1 = \frac{3\sqrt{2}I 2 N_{ph}}{D_{av}\pi} \qquad (11)
$$

If Eq. (11) is substituted in Eq. (10), the torque equation for the basic single stator surface will be as follows:

$$
T_1 = \frac{1}{4}\pi\hat{B}_{g1}k_{\omega1}K_1 D_{av}^2 L_i\sin(\beta) \qquad (12)
$$

If the Eq. (12) is multiplied by the number of the stator h, the torque expression produced on each stator surface is obtained. Similarly, the rms value of EMF induced in one phase is similar to E_{ph} given in Eq. (13). ω_m rotor angular velocity is given in Eq. (13) [20]:

$$
E_{ph} = \frac{\sqrt{2}}{2}\hat{B}_{g1}\omega_m k_{\omega1}N_{ph}D_{av}L_i \qquad (13)
$$

The apparent input power S_{elm} for the stator number h, regardless of the connection status of the stator (series, parallel), is given in Eq. (14) [20]:

$$
S_{elm} = 3hE_{ph}I = \pi\frac{h}{4}\hat{B}_{g1}\omega_m k_{\omega1}K_1 D_{av}^2 L_i \qquad (14)
$$

Another parameter that must be calculated for AF-PMSM is the length and thickness of the magnet to be used. The magnet thickness is defined as h_m, μ_{rec} as the relative permeability of the magnet, B_r as the residual flux density of the magnet, and B_g as the flux density of the air gap.

$$
h_m = \frac{B_g\mu_{rec}g}{\left(B_r - B_g\right)} \qquad (15)
$$

Additionally, in order for the performance curves to be obtained analytically at Line Start AF-PMSM, rotor resistance and leakage inductance values of squirrel cage must be calculated. Fig. 4 demonstrates a squirrel cage designed for an axial flux motor topology.
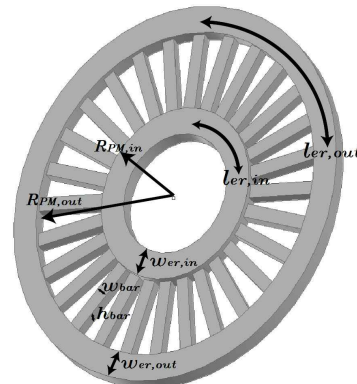

Fig. 4. Generalized squirrel cage for AFSM

The length of the inner and outer of the squirrel cage's ring is calculated with the Eq. (16) [22].

$$l_{er,in} = \frac{2\pi\left(R_{PM,in} - \frac{W_{er,in}}{2}\right)}{2p} = \frac{\pi\left(R_{PM,in} - \frac{W_{er,in}}{2}\right)}{p}$$

$$l_{er,out} = \frac{2\pi\left(R_{PM,out} + \frac{W_{er,out}}{2}\right)}{2p} = \frac{\pi\left(R_{PM,out} + \frac{W_{er,out}}{2}\right)}{p} \qquad (16)$$

The total resistance R_{r1} of the rotor squirrel cage's ring is calculated by Eq. (17). Given σ_{Al} in the equation is the conductivity of aluminum [22];

$$R_{r1} = \frac{1}{\sigma_{Al}}\left(\frac{l_{er,in}}{w_{er,in}h_{er}} + \frac{l_{er,out}}{w_{er,out}h_{er}} + \frac{l_{bar}}{w_{bar}h_{bar}}\right) \qquad (17)$$

At the Line Start AF-PMSM, the torque produced by the magnets varies depending on the equivalent circuit parameters and decreases the asynchronous torque produced by the rotor bars by braking effect [22].

$$T_{braking} = \frac{3pR_s(1-s)^2 E_0^2}{2w_s(1-s)} \frac{R_s^2 + X_{qs}^2(1-s)^2}{(R_s^2 + X_{qs}X_{ds}(1-s)^2)^2} \qquad (18)$$

In the given equation R_s represents stator resistance, s denotes slip, E_0 denotes the induced voltage at synchronous speed, X_{qs} denotes the stator q axis reactance, X_{ds} denotes the stator d axis reactance, w_s denotes the electrical synchronous velocity. It is clear that the braking torque produced by the magnets is directly proportional to the square of the induced voltage. The choice of magnet volume is very important in AF-PMSM since the large selection of magnet volume increases the induced EMF and reduces the line currents and the thermal load of the rotor while increasing the power factor, and increases the motor's maximum output power. However, rising magnet volume increases the braking torque produced and reduces the resulting torque and torque angle. Moreover, if the collapse torque at the starting torque is not well adjusted at the moment of starting, the motor may have a negative impact during acceleration under load [23].

In addition to these values, the inertia moment of the rotor is also affect the efficiency. Therefore, the moment of inertia must be counted. The parameters affecting the rotor inertia moment must be calculated separately. The shaft moment of inertia is [21];

$$J_{sh} = m_{sh}\frac{D_{sh}^2}{8} \qquad (19)$$

The moment of inertia of PMs is

$$J_{PM} = m_{PM}\frac{D_o^2 + D_i^2}{8} \qquad (20)$$

The moment of inertia of backing steel disc is

$$J_{Fe} = m_{Fe}\frac{D_o^2 + D_{sh}^2}{8} \qquad (21)$$

The resultant moment if inertia of the rotor is

$$J_r = J_{sh} + J_{PM} + J_{FE} \qquad (22)$$

m_{sh} is mass of shaft, D_{sh} is shaft diameter, m_{PM} is the mass of all PMs, m_{Fe} is the mass of backing steel disk [21].

3. Design and Result

3.1 Analytical design results

Due to its simple structure and high torque capacity, the single-sided axial flux permanent magnet motor is used in the study. By modifying the rotor architecture, 5.5 kW shaft power, which can be started directly from the line, was designed with an axial-flux permanent magnet motor. Firstly, the motor design was realized analytically according to target values and selected rotor structure. The analytically calculated values of the motor are given in Table 1.

3.2 Magnetic analysis and results

FEM is also used to calculate the flux distribution in the electric machines. The electromagnetic field can be determined by solving the Maxwell equations in a space

Table 1. Calculated values

Motor Parameters	Value	Unit
Stator outer diameter	0.248	m
Stator inner diameter	0.132	m
Stator current	9.43	A
Stator's winding number per phase	38	turns
Back EMF	198	V
Line surge current density	21000	A/m
Magnet thickness	4	mm
Conductor cross section	2x1.151	mm^2
Air gap	1	mm
Stator's winding resistance per phase	0.96	Ω
Resistance of squirrel cage	1.06	Ω
Stator leakage reactance	2.082	Ω
Rotor leakage reactance	0.919	Ω
Inertia moment of rotor	0.10902735	Kg.m^2
Damping factor	0.00162113	Nms/rad
Power factor	0.936	
Output power	5460	W
Input power	5862	W
Efficiency	93.14	%
Electromagnetic torque	35.01	Nm

limited by user defined appropriate initial conditions and boundary conditions. Some equations are given below.

$$\nabla X E = -\frac{\partial B}{\partial t} \tag{23}$$

$$\nabla \cdot B = 0 \tag{24}$$

$$\nabla X H = J + \frac{\partial D}{\partial t} \tag{25}$$

$$\nabla \cdot D = \rho \tag{26}$$

In the given equation is the electric field intensity, is the magnetic flux density, is the magnetic flux intensity, is the surface current density, D is the electric flux density and ρ is volume charge density [24].

From these equations and some hypotheses, the magnetic flux density and current density can be calculated [24].

$$J = \sigma E = -\sigma(\frac{\partial A}{\partial t} + \nabla V) = \nabla X H = \nabla X \frac{B}{\mu} = \frac{1}{\mu}\nabla(\nabla X A) \tag{27}$$

By using Coulomb Gauge,

$$\nabla \cdot A = 0 \tag{28}$$

The computed transient states for the resulting electromagnetic field will be obtained as in Eq. (29) [24].

$$\nabla(\frac{1}{\mu}\nabla X A) = \nabla X H_C - \sigma(\frac{\partial A}{\partial t} + \nabla V) + \frac{1}{\mu}\nabla(\nabla \cdot A) \tag{29}$$

Here A is the magnetic vector potential, H_C is the coercive magnetic field intensity and V is the electrical scalar potential.

The AF-PMSM structure forms the basis of the designed motor structure. It was not changed single-sided AF-PMSM's stator structure and used slotted structure in the traditional stator structure. The innovative aspect of this work was realized in rotor architecture. At the surface mounted rotor structure, the bars were fixed in the slots opening to the rotor core, under the magnets. The magnets were mounted in contact with the rotor core.

The analytically designed single sided The analytically designed single sided Line Start AF-PMSM was analyzed with 3D-FEM to extract the motor characteristic curves. FEM is a numerical technique to solve the integral and differential equations such as fluid dynamics, solid and structural mechanics, electromagnetic, magneto statics and thermal conductivity [25]. The ANSYS program is one of the general purpose finite element package programs used to solve physical problems. ANSYS Electromagnetics Suite 16.0 was performed in the magnetic analysis of the motor. The quarter of a motor model was used to reduce the calculation time for the magnetic analysis. The quarter model and the material of the motor is shown visually in Fig. 5 and Table 2 respectively.
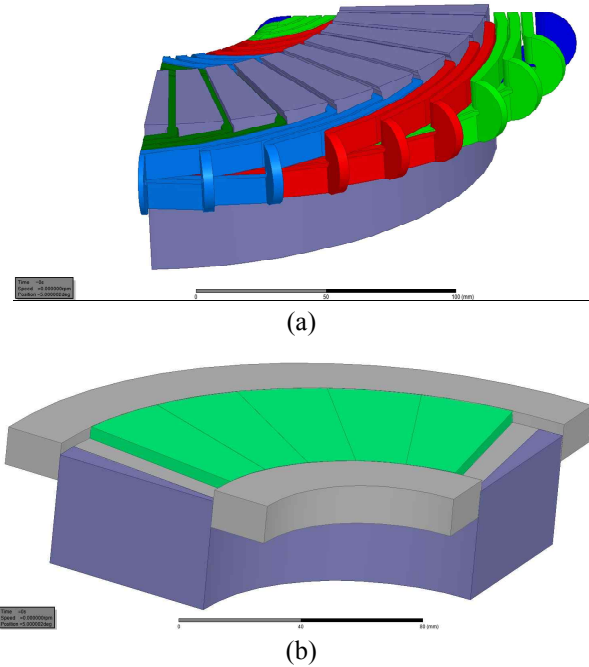

(a)

(b)

Fig. 5. Model of the created architecture (a) stator with windings, (b) rotor

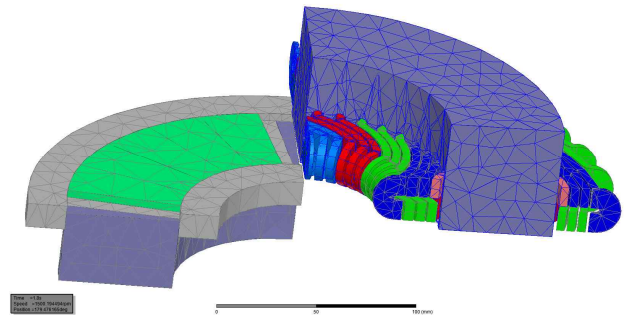**Fig. 6.** AF-PMSM mesh view produced with FEM

Table 2. Material type of Line Start AF-PMSM part

Line Start AF-PMSM part	Material
Stator	JFE_20JNEH1500
Rotor	Steel 1010
Magnet	N45-SH

Maxwell 3D, separates the region into subregions called tetrahedra, which are like a lot of pyramidal elements (tetrahedra) in order to determine electric and magnetic fields in non-uniform geometric regions. The area of each quadruple element is determined by a separate polynomial. The sum of these elements is expressed as the finite element grid or simply grid (mesh). Tetrahedra network structure was used in the analyzes. The number of small regions formed in this structure is directly related to the closeness to the correct result. A total of 37781 regions were created as a result of the mesh processing. While there were consisted totally 12302 regions in stator and windings; 3874 regions were consisted in the rotor, bar and

magnets. The rest of the regions are located in the defined band and study regions.

A 5.5 kW shaft power, 4-poles Line Start AF-PMSM was designed with 3D-FEM and it was started under 100% load (35 Nm load). The designed Line Start AF-PMSM was operated with 0.001 sec time intervals for 1.8 sec under dynamic operating conditions. The dynamic performance of the motor was monitored and parameters such as three-phase stator current, torque, speed, efficiency, the power factor of the motor were obtained. While the analyzes were made, necessary adjustments were made in the FEM program used, the effects of the inertia moment and friction were counted in. A phase stator current, torque and speed curves of the motor are shown in Fig. 7.

As shown in Fig. 7(b), the motor reaches synchronous speed in less than 1.2 seconds. The rms value of the current during the start was determined as 60.49A. After reaching synchronous speed, the rms value of the current in one phase of the motor was determined as 10.43 A. Furthermore,
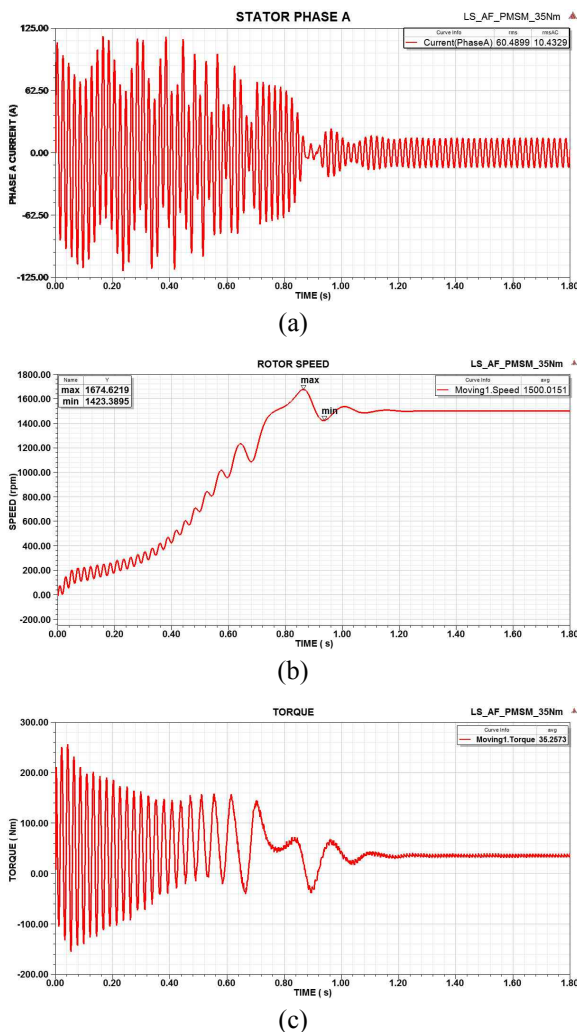
when the speed graph is examined, it can be seen that the motor can be started from the line and if it exceeds the synchronous speed, it can return to the synchronous speed again. The maximum rotor speed was determined as 1675 rpm. After the rotor speed reaches its maximum value, the rotor's speed drops to 1422 rpm. After reaching the motor synchronous speed, the average value of the rotor speed was determined as 1500 rpm. Although there is a large ripple in the electromagnetic torque, the average torque is 57.12 Nm. In other words, motor is accelerating with positive average torque. The average torque value of the motor after synchronization is 35.26 Nm. In Fig. 8-10 the efficiency, power factor and torque ripple graphs are given according to motor shaft power changes.

The average value of motor efficiency, where the shaft power is between 1500W and 6250W, is 93.22%. The Line Start AF-PMSM operates at 93.14% efficiency under full load. If the motor is above the nominal load value, the motor efficiency value decreases to 92%. Fig. 10 shows a graph of shaft power factor change. When the motor is
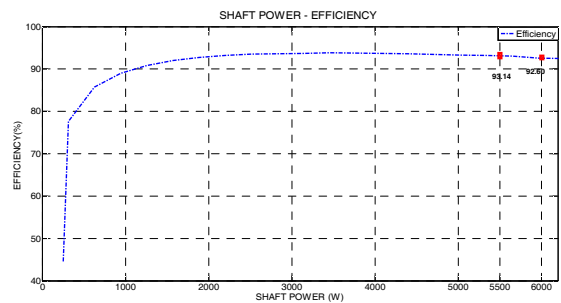

(a)

(b)

(c)

Fig. 7. ANSYS Electromagnetics Graphs (a) Current Time Graph, (b) Velocity Time Graph, (c) Torque Time Graph)
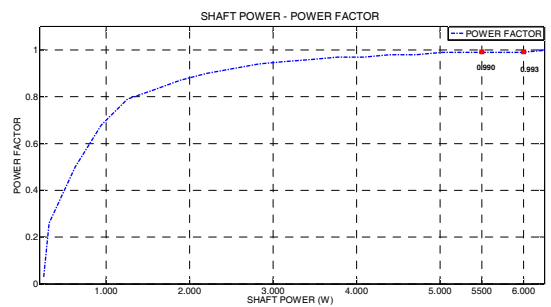

Fig. 8. Motor efficiency according to the shaft power

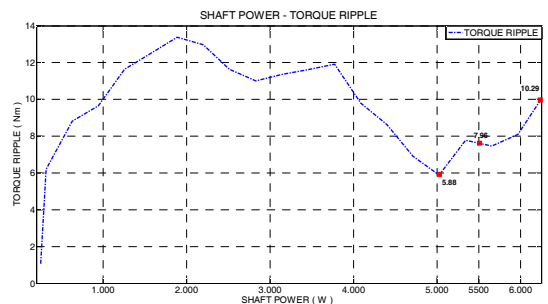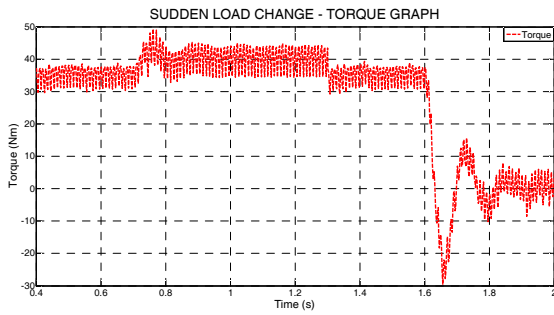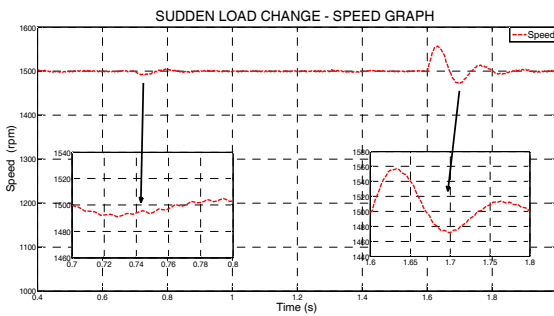**Fig. 9.** Power factor according to the shaft power

Fig. 10. Torque ripples according to motor shaft power

(a)

(b)

Fig. 11. Sudden load changes graphs (a) Torque (b) Speed)

operating under full load the power factor is 0.989. While operating at nominal load, power factor values vary between 0.970–0.995. These results indicate that the motor is very close to the ohmic operating point. Torque ripple affects the motor performance even in axial flux motors as is in radial-flux permanent magnet motors. It is seen that the back EMF, which is not ideal for torque ripple, causes torque to cogging and saturation of magnetic circuits. Thanks to the changes made in the motor architecture, these torque ripples can be reduced. At the end of the analyses performed with FEM, it was seen that the ripple of torque under full load in Line Start AF-PMSM was 7.96 Nm and it was determined as 10.29 Nm under 125% load. These values are acceptable for surface mounted PSMSs.

In order to obtain synchronization capability of the Line Start AF-PMSM, sudden load torque change test was implemented with FEM and obtained results were given in Fig. 11.

In this test, first of all, the full load (nominal load) of the motor was applied while the motor was operating with no load. In this situation, although the motor speed decreases under synchronous speed, it was synchronized again in a shorter time which is 0.1 sec. Secondly, the load was removed suddenly. In this case, the motor was synchronized if there were speed oscillations.

3.3 Thermal analysis and results

Another process needs to be done on the motor to reach the desired data from the electromagnetic analysis is thermal analysis. Thermal analysis is vital for motors
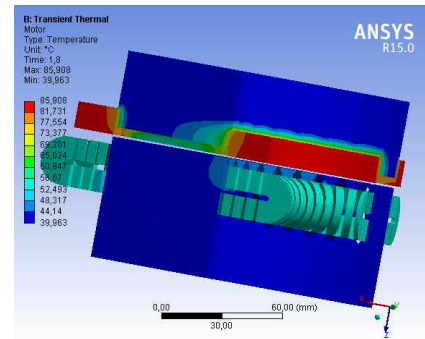

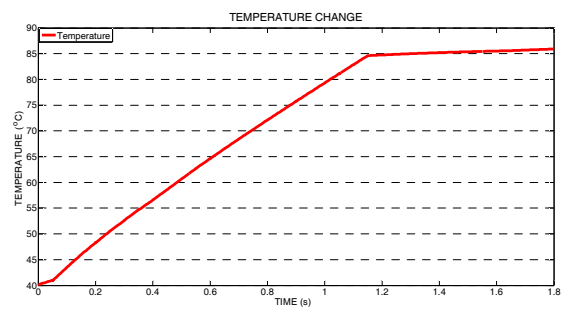**Fig. 12.** Line Start AF-PMSM thermal analysis result of the temperature distribution

Fig. 13. Line Start AF-PMSM thermal analysis result of temperature change

Table 3. Minimum and maximum values of temperature distribution according to motor parts

Line Start AF-PMSM Part	Minimum Temperature (^{0}C)	Maximum Temperature (^{0}C)
Stator	40.00	50.97
Stator Windings	42.06	55.57
Rotor	**39.96**	82.43
Magnet	43.16	81.43
Squirrel Cage	58.32	**85.91**

containing magnets. Increasing the temperature of the motor can cause demagnetization fault on the magnets. Demagnetization fault reduces the flux obtained from the magnet, so it negatively influences the efficiency. In case of overheating, it will also increase the loss due to temperature.

Materials used in the motor were selected from standard industrial materials like steel, copper, aluminum. In the thermal analyzes made, the thermal properties and coefficients of the materials were obtained from literature review and material catalog data. AF-PMSM was analyzed under dynamic operating conditions, defining the thermal properties of materials to the ANSYS Electromagnetics Suite 16.0 program. In this way, the thermal losses occurring in the materials were obtained quantitatively.

The obtained results were transferred to ANSYS Workbench 15.0 interface. In ANSYS Workbench 15.0 program, the thermal properties of the motor parts and the contact surfaces were identified and thermal analysis was

performed. Ambient temperature is defined as 40°C. Fig. 12 shows the temperature distribution which is the result of the Line Start AF-PMSM thermal analysis.

As shown in Fig. 12-13 and Table 3, the maximum temperature the motor reaches is 85.91 ° C. This value was obtained in the squirrel cage. The highest temperature values were obtained in the magnet and rotor parts that come into contact with the squirrel cage. In prototype motor, N45-SH type magnets are used, so the demagnetization temperature for this magnet started from 150°C. With the values obtained with 3D-FEM, the magnet temperature increased to 81.43°C. This value is the suitable temperature value for the used magnet. The temperature values of the stator and its windings are in the acceptable range. The results demonstrate that there is no thermal obstacle in the Line Start AF-PMSM design.

3.4 Structural analysis and results

Another analysis that needs to be done in the model, where the electromagnetic and thermal analysis is completed, is the structural analysis of the motor. The physical characteristics of the materials of the Line Start AF-PMSM have been defined by creating solid models in the ANSYS Workbench 15.0 interface. The operating speed of the designed Line Start AF-PMSM is 157.08 rad/s. The motor has defined forces that will act in terms of centripetal acceleration. Fig. 14 shows the rotational velocity graph of the motor.

Total Deformation, Equivalent (von-Mises) Stress and Shear Stress parameters were examined through structural
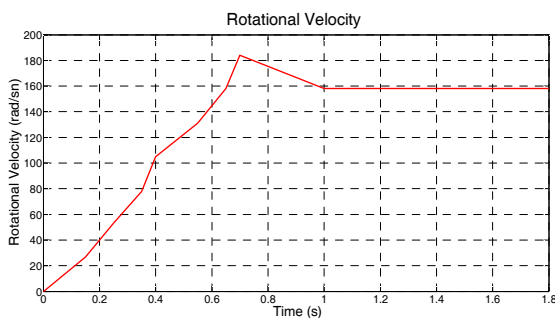
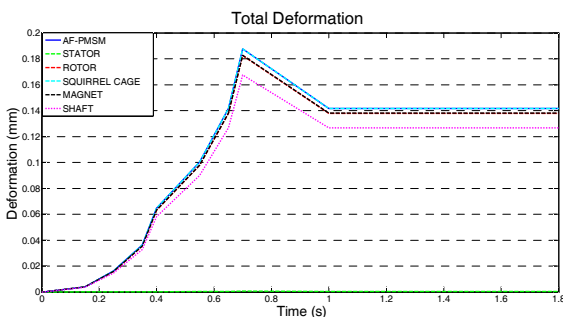analysis. First, the total deformation, which is the displacement of the material under load, was investigated. The maximum displacement of the motor parts was determined as 0.187 mm. It is estimated that the obtained value is a negligible value like 0.19%. Axial deformation is an important part of the total deformation in the axial flux motors. The change in the air gap size, in which energy conversion occurs, affects the motor parameters. The displacement observed in the Z-axis direction was 0.0007 mm. This value is negligible. The graphs of total deformation coming from the motor are shown in Fig. 15 and Fig. 16.

Other parameters examined in structural analysis are shear stress and equivalent stress values. These values relate to plastic deformations that occur in the material. The places where equivalent stress and shear stress occur are overlapped. Plastic deformation was not observed in the materials because the analysis was smaller than the yield strength at this value. It has been observed that the materials used in the motor do not constitute any risk.

4. Conclusion

The importance of energy efficiency has increased day by day. When the share of electric motors' energy consumption in total energy consumption is considered, the
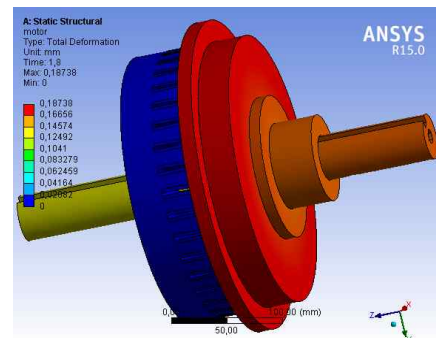
(a)
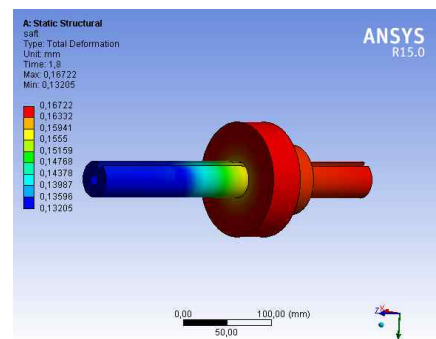
(b)

Fig. 16. ANSYS graphics of total deformation occurred in the motor

Fig. 14. Defined rotational velocity graph

Fig. 15. Total deformation occurred in motor parts

importance of efficiency of these motors can clearly be seen. In this study, an AF-PMSM was designed with a squirrel cage attached to the rotor to allow direct delivery from the line. In applications requiring constant speed, lift systems and fan applications can be used instead of asynchronous motors with higher efficiency and higher power factor. The efficiency is 3%-4% higher than an asynchronous motor with the same power, and this value gives a significant advantage in the total cost of consumption of electric motors. In addition, this structure can be connected to network directly does not need a comprehensive driver like other PM motors. This feature makes L and S AF-PMSM more advantageous than other PM motors. Furthermore, due to the advantages provided by the axial flux structure, it is thought that it can be preferred more than the line start radial flux PMSMs on the mains. The design of Line Start AF-PMSM with 4 poles, 5.5 kW power, and 1500 rpm rotational speed is realized. As a result, an electric motor class IE4 with an efficiency of 93%. 14 and a power factor of 0.989 is obtained. These values show that the design targets are achieved. This hybrid motor will be a good alternative for asynchronous motor and radial flux PMSM in industrial applications. The prototype motor will be manufactured in the next stage and the experimental results will be compared with the FEM model results. The text must include a citation of each figure and table.

References

[1] Mohamed Benhaddadi, Jean-F. Landry, Ronald Houde and Georges Olivier, "Energy Efficiency Electric Premium Motor-Driven Systems," *in: International Symposium on Power Electronics, Electrical Drives, Automation and Motion (SPEEDAM),* Sorrento, Italy, pp. 1235-39, Aug. 2012.

[2] Vera Elistratova, "Optimal Design of Line-Start Permanent Magnet Synchronous Motors of High Efficiency, (Ph.D. Thesis)," *PRES Université Lille Nord-de-France: France*; 2016.

[3] Güvenir K. Esen, "Energy Consumption of Electric Motors and Related Technical Legislation in Turkey and the World," http://www.emo.org.tr/ekler/ *364734147179187_ek.pdf*, 2015 [accessed 02.06.2017].

[4] Anibal T. Almeida and Fernando J.T.E. Ferreira, Ge Baoming, "Beyond Induction Motors-Technology Trends to Move up Efficiency," *IEEE Transactions on Industry Applications*, vol. 50, no. 3, pp. 2103-14,

June 2013.

[5] Edgar P. Sanchez and Andrew C. Smith, "Line-Start Permanent-Magnet Machines Using a Canned Rotor," *IEEE Transactions on Industry Aplications*, vol. 45, no. 3, pp. 903-10, 2009.

[6] Hamidreza Behbahanifard and Alireza Sadoughi, "Line Start Permanent Magnet Synchronous Motor Performance and Design; a Review," *J. World. Elect. Eng. Tech.*, vol. 4, no.2, pp. 58-66, Dec. 2015.

[7] Erol Kurt, Halil Gör and Mehmet Demirtas, "Theoretical and Experimental Analyses of a Single Phase Permanent Magnet Generator (PMG) With Multiple Cores Having Axial and Radial Directed Fluxes," *Energy Conversion and Management*, vol. 77, no. 2014, pp. 163-72, Jan 2014.

[8] Myung K. Seo, Tae-Yong Lee, Kyungsoo Park, Yong-Jae Kim and Sang-Yong Jung, "Characteristic Analysis and Experimental Verification of the Axially Asymmetric Structured Outer-Rotor Type Permanent Magnet Motor," *J Electr Eng Technol.*, vol. 11, no.4, pp. 898-904, 2016.

[9] Ferhat Daldaban and Emrah Çetin, "Prototyping of Axial Flux Permanent Magnet Motors," *in: 3rd International Symposium On Innovative Technologies In Engineering And Science (ISITES)*, Universidad Politecnia de Valencia, Spain, pp. 90-96, July 2015.

[10] Engin Huner and Mustafa C. Aküner, "Axial-Flux Synchronous Machines Compared with Different Stator Structures for Use in Working," *Przeglad Elektrotechniczny*, vol. 11, no. 11a, pp. 174-77, 2012.

[11] Mustafa C. Aküner and Engin Hüner, "The Air Gap and Angle Optimization in The Axial Flux Permanent Magnet Motor," *Electronics and Electrical Engineering*, vol. 17, no. 110, pp. 25-29, 2011.

[12] Solmaz Kahourzade, Amin Mahmoudi, Hew W. Ping and Mohammad N. Uddin, "A Comprehensive Review of Axial-Flux Permanent-Magnet Machines," *Canadian Journal of Electrical and Computer Engineering*, vol. 37, no. 1, pp. 19-33, 2014.

[13] Asko Parviainen, "Design of Axial-Flux Permanent-Magnet Low-Speed Machines and Performance Comparison Between Radial-Flux and Axial-Flux Machines(Ph.D.Thesis)," *Lappeenranta, Lappeenranta University of Technology, Finland*, 2005.

[14] Fabio G. Capponi, Giulio D. Donato and Federico Caricchi, "Recent Advances in Axial-Flux Permanent-Magnet Machine Technology," *IEEE Transactions On Industry Applications*, vol. 48, no. 6, pp. 2190-205, Nov.-Dec. 2012.

[15] Harri Hakala, "Integration of Motor and Hoisting Machine Changes the Elevator Business," *in: Proceedings International Conference Electrical Machines*, Espoo, Finland, vol. 3, pp. 1242-45, 2000.

[16] Francesco Profumo, Zheng Zhang and Alberto Tenconi, "Axial Flux Machines Drives: a New Viable Solution for Electric Cars," *IEEE Transactions on Industrial*

Electronics, vol. 44, no. 1, pp. 39-45, Feb 1997.

[17] Fabrice Locment, Eric Semail and Francis Piriou, "Design and Study of a Multiphase Axial-Flux Machine," *IEEE Transactions on Magnetics,* vol. 42, no. 4, pp. 1427-30, Apr. 2006.

[18] Metin Aydin, Surong Huang and Thomas A. Lipo, "Torque Quality and Comparison of Internal and External Rotor Axial Flux Surface-Magnet Disc Machines," *IEEE Transactions on Industrial Electronics*, vol. 53, no. 3, pp. 822-830, Jun. 2006.

[19] Petr Chlebis, Ales Havel and Petr Vaculik, "The Design of HEV Drive Unit with an Axial Flux Rotary Converter," *in Proc. Progress In Electromagnetics Research Symposium Proceedings*, KL, MALAYSIA, pp. 987-90, Jan. 2012.

[20] Funda Sahin, "Design and Development of a High-Speed Axial-Flux Permanent Machine, (Ph.D. Thesis)," *Eindhoven: Technische Universiteit Eindhoven,* 2001.

[21] Jack F. Gieras, Rong-Jie Wang and Maarten J. Kamper, "Axial Flux Permanent Magnet Brushless Machines," Kluwer Academic Publishers Dordrecht, 340 p, United States of America, 2004.

[22] Janne Kinnunen, "Direct On Line Axial Flux Permanet Magnet Synchronous Genarator Static and Dynamic Performance, (Ph.D. Thesis)," *Lappeenranta University of Technology*, 2007.

[23] Gosenay Hatik, Elif İngenç and Mehmet Akar, "Investigate of the Rotor Bar Failure in Line Start Permanent Magnet Syncnhronous Motors," *in Proc. 2nd International Symposium on Innovative Technologies in Engineering and Science*, Karabuk University, Karabuk, Turkey, pp. 1381-88, 2014.

[24] X. Ge, "Simulation of Vibrations in Electrical Machines for Hybrid-Electric Vehicles, (Master's Thesis)," *Chalmers Unıversity of Technology Göteborg, Sweden*, 2014.

[25] Jawad Faiz and Bashir Mahdi Ebrahimi, "Locating Rotor Broken Bars in Induction Motors Using Finite Element Method," *Energy Conversion and Management*, vol. 50, no. 1, pp. 125-131. Jan. 2009.

Mehmet Akar was born in Tokat, Turkey, in 1979. He received the B.S. and Mc. S. degree in electrical education from Marmara University, Technical Education Faculty, Istanbul Turkey, and he received the Ph.D. degree in electronic and computer education from the University of Sakarya, Sakarya, Turkey in 2002, 2005 and 2009, respectively. He is currently an Associate Professor Mechatronics Engineering Department in Gaziosmanpasa University. His research interests include electrical machines design, control and fault diagnosis.

Mustafa Eker was born in Tokat, Turkey, in 1985. He received the Bachelor's degree in electrical and electronics engineering from Bulent Ecevit University and the Ph.D. degree in Mechatronics Engineering from Gaziosmanpasa University, in 2013 and 2018, respectively. He is currently as an assistant professor at Gaziosmanpasa University. His research interests focus on electrical machines design and fault diagnosis.

Cem Emeksiz obtained his Bachelor's degree in Electronic Engineering from the Erciyes University, Kayseri, Turkey in 1999. He received the M.S. degree in institute of science from the Gaziosmanpasa University, Tokat, Turkey; 2007 and the Ph.D. degree in solar energy institute from Ege University, Izmir, Turkey; 2014 respectively. He was appointed as Assistant Professor in 2014, in the Department of Electrical and Electronics Engineering, Faculty of Natural Sciences and Engineering Gaziosmanpasa University, Tokat, Turkey. His research interests Renewable Energies, Wind energy, Solar Energy, Superconductors, Digital Electronics.

Zafer Dogan was born in Tokat, Turkey, in 1974. He received the B.S. and Mc. S. degree in electrical education from Marmara University, Technical Education Faculty, Istanbul Turkey, in 1996 and 2009, respectively. He is currently a assistant professor in the Department of Electrical and Electronics Engineering, Gaziosmanpasa University Faculty of Engineering and Natural Sciences. His research interests are design of electrical machines and fault diagnosis in electrical machines.

Ahmet Fenercioglu, He received B.S and M.Sc. degrees in Electrical Education in 1994 and 1996 respectively from Marmara University, Turkey. He received Ph.D. degree in electrical machinery main field in 2006 from Gazi University, Turkey. He is currently as an associate professor in Mechatronics Engineering Department at Gaziosmanpasa University. His major research interests are electro-mechanical systems and design of electrical machinery.